J. Webster (ed.), *Wiley Encyclopedia of Electrical and Electronics Engineering*

OPTICAL INFORMATION PROCESSING

Information-processing techniques that exploit the capabilities of optical hardware offer many advantages. These include high-speed parallel processing, large-volume data handling, compactness, low power consumption, and ruggedness (1,2,3,4,5,6,7,8,9,10,12). Compact custom-made optical hardware can process two- dimensional arrays of data of up to half a million pixels at kilohertz frame rates. Most applications of optical processing systems have been for military hardware because of high cost and performance demands. Recent advances in optical material devices and components, such as optical memory and optical display devices, have made optical information-processing systems more attractive for commercial applications. In addition, many of the innovative algorithms developed in the context of optical information processing can also be implemented on a digital computer and perform well compared to various algorithms developed by the digital signal-processing community.

This article presents a brief review of the fundamentals of optical information processing. We discuss optical information-processing techniques, materials, and devices for optical processing, pattern recognition, and memory and their applications to optical encryption, security, and anticounterfeiting. Optical image-processing algorithms and architectures, as well as basic hardware concepts such as the fundamentals of optical spatial light modulators, are reviewed. A short bibliography on these topics is included.

Fundamentals

The Fourier transform of an image can be optically generated in the space domain by using a lens (1,2,3,4,5). As a result, various image-processing algorithms can be implemented. The complex amplitude of the light distribution $E(\alpha, \beta)$ at the back focal plane of a lens is the two-dimensional Fourier transform of the light transmittance in the front focal plane [Fig. 1(a)]. This Fourier-transform relationship is the fundamental relationship in the analysis of optical processors. If a second lens, L2, is placed behind the Fourier plane as shown in Fig. 1(b), the light distribution at the back focal plane of L2 is the double Fourier transform of the input field.

A spatial filter can be placed at the Fourier plane to produce different image-processing operations. A complex spatial filter $F(\alpha, \beta)$, where $F(\alpha, \beta)$ is the Fourier transform of $f(x, y)$, can be inserted at the Fourier plane, resulting in the light field $F(\alpha, \beta)E(\alpha, \beta)$ leaving the filter plane. Therefore, at the output plane P3 we obtain the Fourier transform of $F(\alpha, \beta)E(\alpha, \beta)$, which is equivalent to the convolution of the input signal $e(x, y)$ with the filter function $f(x, y)$. In the input plane, a particular component of a convolution function is the integral of an input signal multiplied by a filter function rotated 180° at a particular position. A correlation is the same operation without the 180° rotation, which implies that high-correlation peak values are obtained when the input signal is very similar to the filter function.

Numerous signal- and image-processing operations can be performed by using an appropriate spatial filter. One such operation—correlation filtering—is shown in Fig. 1(b). Optical decryption via spatial filtering is shown in Fig. 1(c). Optical encryption will be discussed later.

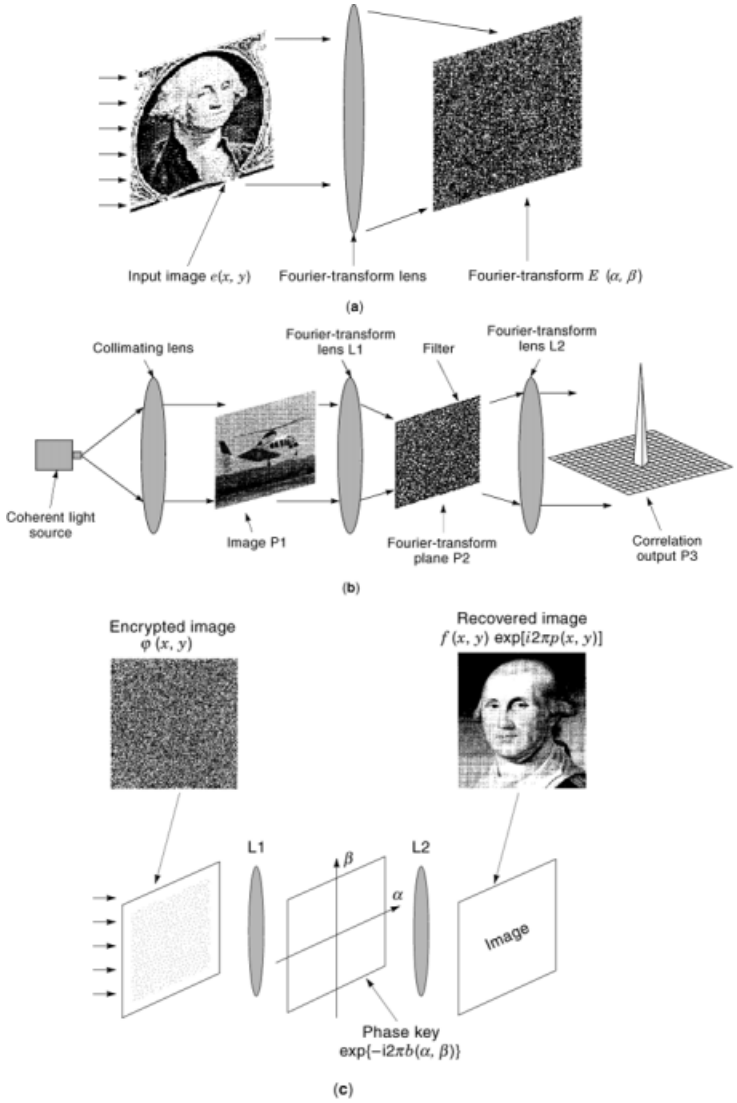

Fig. 1. (a) Fourier transform property of a lens. (b) Optical information-processing system. Plane (α, β) is the Fourier plane, where a filter function can be inserted to execute different image processing operations. (c) Optical system used for decryption. The encrypted image is inserted at the input plane and the key for decryption, $\exp[-i2\pi b(\alpha, \beta)]$, is inserted at the Fourier plane. The decrypted image is recovered at the output plane. An example of the decrypted image is shown using the correct key.

There are a number of ways to synthesize an optical filter. A computer can be used to generate and write the spatial filter onto an optical display device in the Fourier plane. Holographic techniques can also be used to generate the spatial filter. Figure 2 shows a holographic technique to synthesize an optical matched spatial filter (1, 2, 9). The matched filter is designed to detect a specific image or target in the presence of noise. For white noise, the matched filter is simply the target itself in the spatial domain. In the Fourier domain it is

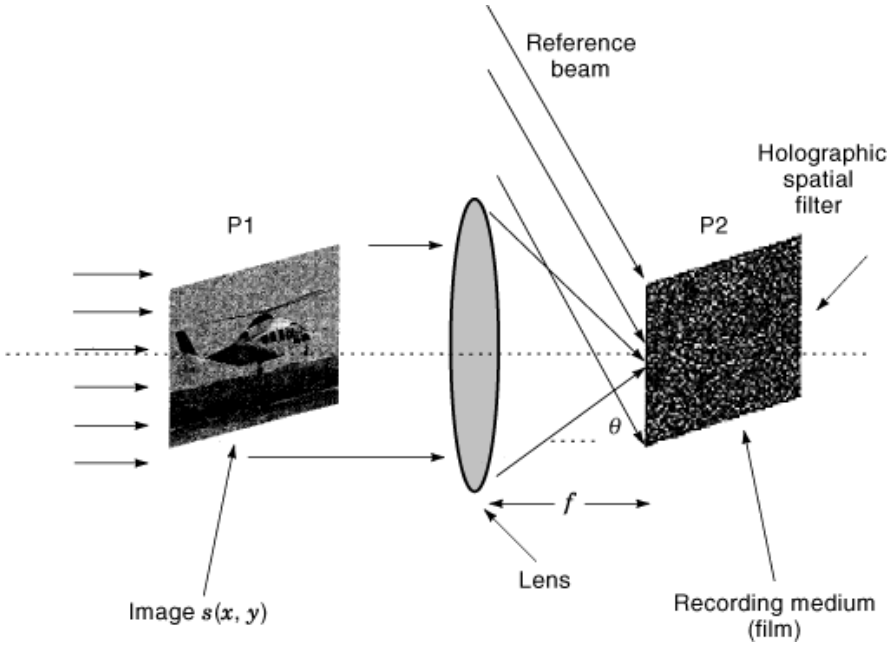

Fig. 2. Interferometric holographic technique for synthesizing an optical spatial filter.

equal to the complex conjugate of the Fourier transform of the target. For a reference signal $s(x, y)$, its matched spatial filter $S*(\alpha, \beta)$, where the asterisk denotes complex conjugation, is produced at the filter plane P2.

The reference signal $s(x, y)$, is inserted at the input plane P1 as shown in Fig. 2. The light distribution $S(\alpha, \beta)$ at the filter plane P2 is the Fourier transform of the input reference signal $s(x, y)$. Incident on the plane P2 at an angle θ with respect to the optical axis is a plane-wave reference beam of uniform amplitude. A conventional holographic technique is used to record the interference patterns of the reference signal Fourier transform $S(\alpha, \beta)$ with the reference beam. This produces the matched filter at the Fourier plane for detecting the reference signal $s(x, y)$. The hologram is recorded by placing a detector, such as high-resolution photographic film or a photosensitive recording material, at plane P2. The intensity distribution at the filter plane is obtained when the film is developed to produce a filter transmittance function, which includes the desired matched spatial filter of $s(x, y)$. This is proportional to the complex conjugate of the reference signal's spectrum $S*(\alpha, \beta)$.

If the matched spatial filter just described is placed at the Fourier plane and an arbitrary signal $g(x, y)$ is inserted at the input plane, the complex amplitude of the light leaving the filter plane is the product of the filter's transmittance function and the input signal's spectrum: $S*(\alpha, \beta)\, G(\alpha, \beta)$. This is shown in Fig. 1(b). Plane P2 is located at the front focal plane of lens L2 as shown in Fig. 1(b), which processes the light leaving the plane P2 to produce its Fourier transform in plane P3. Since the product $S*(\alpha, \beta)\, G(\alpha, \beta)$ in the Fourier plane is equivalent to a correlation in the input plane, the light pattern in the output plane P3 is proportional to the cross-correlation between the input signal $g(x, y)$ and the reference signal $s(x, y)$.

Spatial Light Modulators

Spatial light modulators (SLMs) are used in optical computing systems, programmable optical interconnects, optical neural networks, and optical pattern recognition systems (1,2,3,4,5,6,7,8). The SLM input is either a

light distribution, such as an image, or a time-dependent electric signal. SLMs with optical or electrical input are called optically and electrically addressed SLMs, respectively. The SLM modulates the amplitude and/or phase, or polarization of the read-out light beam as a function of the input signal. The writing light $A_i(x, y)$ is incident on the input of the SLM. This is generally a two-dimensional spatially varying amplitude distribution, imaged onto the input of SLM. The output light distribution is a function of the input light amplitude $A_i(x, y)$.

There are many types of SLMs, such as a liquid crystal light valve (LCLV), liquid crystal television (LCTV), nematic liquid crystal (NLC) devices, ferroelectric liquid crystal (FLC) devices, microchannel SLMs, deformable mirror devices, digital micromirror devices, Pockels' read-out optical modulator (PROM), preobrasovatel izobrazheniy (PRIZ), multiple-quantum-well (MQW) SLMs, and magneto-optical SLMs (1,2,3,4,5,6,7,8). SLMs can act as transducers and convert incoherent light to coherent light, provide input image amplification, convert wavelength, and reverse contrast. They can be used to perform arithmetic operations, including addition, subtraction, multiplication, and division. Many SLMs also possess nonlinear transfer characteristics. SLMs have memory that enables short-term storage, information latching, and low-level signal integration. In the following sections, we will explain how SLMs are used in optical information processing.

Various SLMs differ in addressing methods and the modulating materials used. The input light may be converted to an electric field distribution by a photoconductor, or the electric field can be directly applied using transparent conductive electrodes. The electric field modifies the properties of the modulating material; for example, it may change the optical refractive index. The read-out image is created by modulating the read-out light beam with the modulating element and reflecting it back. Some modulating properties are the electro-optic effect, molecular alignment by an electric field that exists in liquid crystals, the photorefractive effect, electrostatic deformation, and the acousto-optic effect.

SLMs are used to perform various functions in optical systems. These include converting incoherent into coherent light for converting real scenes illuminated under natural or other incoherent light into a coherent image. For real-time Fourier plane spatial filtering, spatial filters can be displayed on SLMs in the Fourier plane. This method can be used in optical spatial filtering, pattern recognition, neural networks, and encryption.

SLMs can also be used for real-time holography. The interference generated between the object and reference beams can be positioned on an optically addressed SLM. Thus the holographic pattern can be displayed on the SLM. SLMs can store data or images as well. This is useful for optical memory, database or knowledge-based processors, pattern recognition, neural networks, and encryption.

SLMs can be used to nonlinearly transform an image or create a binary image. This property is useful for logic operations and switching in digital optical computing (2, 3). In information processing, nonlinear characteristics of the SLM can be used for nonlinear filtering and nonlinear signal processing (11) (see Chap. 4 of Ref. 6).

Many criteria are considered when designing and using an SLM for optical processing. The frame rate determines how fast an image can be updated. The spatial resolution is a measure of how much detail can be displayed on an SLM. The space–bandwidth product is a measure of the number of available pixels. The dynamic range is the number of gray levels represented by each pixel. The contrast ratio is the ratio of the maximum to minimum output light level. When precise phase information is critical, it is important for the mirrors or windows of the SLM to be flat to within a fraction of a wavelength of the light. The nonlinear input–output characteristics of SLMs are often considered for specific image-processing applications. The read-out light efficiency and exposure sensitivity define the light budget of the system. SLMs also have electric driving signal power requirements and a write-in and read-out wavelength range.

The liquid-crystal television screen is an example of an electrically addressable SLM. Small television sets, television projectors, and laptop computers widely utilize liquid-crystal devices (2). Owing to their low cost and commercial availability, these displays have been used in the optical signal-processing community for the last several years (10). The liquid-crystal displays used in liquid crystal TVs were not originally designed for coherent optical systems. The surface rouhgness of these devices and the nonuniform phase variation of materials make their optical quality nonideal for coherent systems. However, recent experiments show that

liquid-crystal TV is actually a good device for applications in which an electrically addressable device is needed, and cost is an important factor.

In a liquid-crystal TV, the liquid-crystal display consists of a 90° twisted liquid-crystal layer sandwiched between two polarizers with parallel polarization directions. A detector array can be used to convert the image into array of electric voltages. A transparent conductive electrode on each side of the liquid-crystal layer is used to apply the electric field to the liquid crystal. These electrodes are pixelated and can be electrically addressed. When no electric field is applied, the orientation of the input light is rotated by 90° from one side of the liquid-crystal layer to the other side. This results in no light passing through because the two polarizers are parallel. When an electric field is applied, the twist and tilt of the liquid-crystal molecules are altered depending on the voltage across the liquid crystal layer. As a result, a fraction of the light passing through the liquid crystal layer retains the same polarization as the input light, and therefore, passes through the second polarizer. The fraction of light passing through the display is proportional to the voltage applied to the liquid-crystal layer. Liquid-crystal displays used in projector-type liquid-crystal TVs operate at TV frame rates and typically have about 1000×1000 pixels.

A variety of other optical materials can be used for information processing. Photorefractive materials can store optical images using variations in the index of refraction through the electro-optic effect (1, 2, 6, 11). Upon exposure to a light beam or an image, a photorefractive material produces a spatially-dependent electric field that changes the material's refractive index through the electro-optic effect. These variations in the index of refraction result in the refraction or diffraction of light. An optical beam can be used to read out an image stored in the photorefractive material. Note that the read-out process will degrade a stored image, but techniques exist to make this degradation very small. For a one-dimensional signal with no applied field, the change in the index of refraction $\Delta n(x)$ as a function of the input intensity $I(x)$ is $\Delta n(x) = -K\Delta I(x)/I(x)$, where $\Delta I(x)$ denotes the change in input intensity, and K is a constant dependent on the electro-optic coefficient, refractive index of the material, temperature, and electron mobility. Photorefractive materials are used in optical storage and memory, real-time optical information processing, programmable interconnects, neural networks, holography, distortion compensation, phase conjugation, and encryption.

Spatial filters and holograms can be generated in real time using photorefractive devices. An image $I(x, y)$ is spatially mixed with a reference beam and their interference intensity is recorded in a photorefractive device. The interference intensity changes the refractive index $\Delta n(x, y)$, which is stored in the form of a volume phase hologram. When the device is illuminated by the reference wave, the object beam $I(x, y)$ is reconstructed. The Fourier transform of $I(x, y)$ is stored in the device as a filter function to be used for spatial filtering.

We have discussed two-dimensional spatial optical processors that modulate the information of the light beam using spatial light modulators. Another class of optical processing spatial systems exist that are basically one dimensional and use ultrasound or acousto-optical principles to perform signal processing of temporal data (12,13,14,15,16,17,18,19,20).

We will first consider the basic acousto-optic modulator, the device that impresses an electric signal on a beam of light. This is shown in Fig. 3. The transducer, which launches an acoustic wave into the medium above, is typically a piezo-electric crystal. The acoustic wave induces compression and rarifaction into the medium thus modulating its index of refraction. Hence the medium becomes in effect a moving phase grating that diffracts the light incident on the device from the left. The upper end of the device usually contains an absorbent material to quench the incident wave and prevent reflections and standing waves that could impair the operation of the device. Note that the device is inherently one dimensional, in contrast to a SLM, which is two dimensional. The number of distinct signal elements (so-called space–bandwidth product) in currently available devices is about a few thousand. In the next section we will explain how these devices can be used for detecting signals in the time domain by correlation.

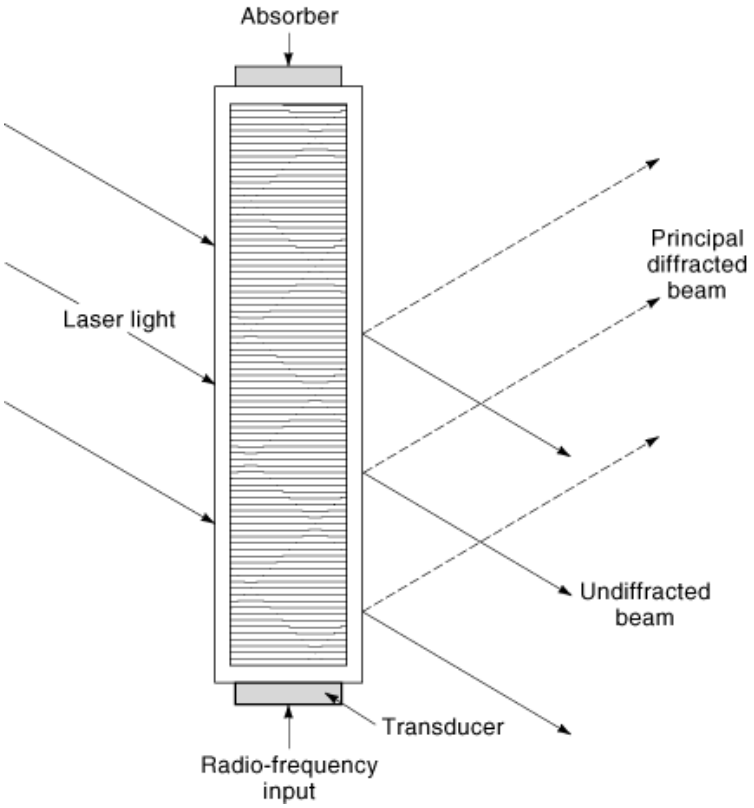

Fig. 3. Acousto-optic cell.

Optical Pattern Recognition

In this section we briefly discuss some algorithms and systems for optical pattern recognition. Much research has been done in this area over the past 20 years. We refer the reader to the references cited for more details (1, 5,6,7, 12,13,14,15,16,17,18,19,20,21,22,23). The matched filter (24) has been extensively used for extracting radar returns for noisy backgrounds. When the input signal is corrupted by additive overlapping Gaussian noise, the matched filter provides the optimal theoretical response of a linear filter. In the derivation of the matched filter, "optimal" is defined as maximizing the signal-to-noise ratio (SNR). It is important to note that there are several different definitions of SNR. In the matched-filter derivation, the SNR is defined as the ratio of the output signal peak to the root mean square of the output noise.

The definition of "optimum" and the fact that the noise overlaps or blankets the target or the signal are very important (25) (see Chap. 1 of Ref. 6). The matched filter is no longer optimum if different design criteria are used. In many pattern-recognition applications the input scene noise does not overlap the target (sometimes called disjoint noise). This means that the scene noise is in the background and thus is partially occluded by the target. For this class of problems, the matched filter and the optimum filter derived under the overlapping input target and scene noise assumption may not perform well (see Chap. 1 of Ref. 6).

Recently, algorithms have been developed for detecting a target in the presence of both nonoverlapping scene noise and additive noise. One approach is to use multiple-hypothesis testing to design an optimum receiver (see Chap. 1 of Ref. 6). It can be shown that for a noise-free target, the optimum receiver is similar to a

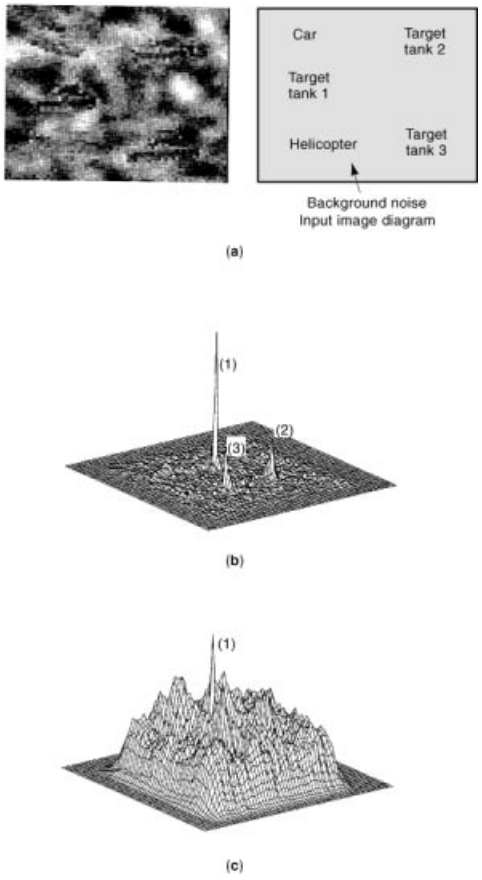

Fig. 4. Performance of the optimum filter for detecting noisy targets in background noise (25): (a) Input scene where three target tanks and two objects (a vehicle and a helicopter) are embedded in white Gaussian-distributed background noise with mean of $m_b = 0.4$ and standard deviation of $\sigma_b = 0.3$. Target tank 1 is identical to the reference tank used in the filter design. Target tank 2 is rotated by 4°. Target tank 3 is scaled up by 10%. The noise added to the targets has mean $m_r = 0$ and standard deviation $\sigma_r = 0.2$. (b) Correlation output of the optimum filter. (c) Output of the matched filter that fails to detect the target.

correlator normalized by the input scene energy within the target window. Interestingly, for situations where the target is noise-free, the detection process is invariant to the scene noise.

Another approach is to design a filter that minimizes the peak-to-output energy (see Chap. 1 of Ref. 6). This is defined as the ratio of the square of the expected value of the output signal at the target location to the expected value of the average output signal energy. Therefore this filter produces a sharp output signal at the target location combined with a low-output-noise floor. Figure 4(a) shows three target tanks and two objects (a vehicle and a helicopter) embedded in white Gaussian-distributed background noise with a mean of $m_B = 0.4$ and standard deviation of $\sigma = 0.3$. Target tank 1 is identical to the reference tank used in the filter design. Target tank 2 is the reference tank rotated by 4°. Target tank 3 is the reference tank magnified by 10%. The optimum filter response to the input shown in Fig. 4(a) is plotted in Fig. 4(b). This compares well with the response of the conventional matched filter in Fig. 4(c). Note that the peak-to-sidelobe ratio is defined as the correlation peak intensity to the largest noise peak intensity at the output plane.

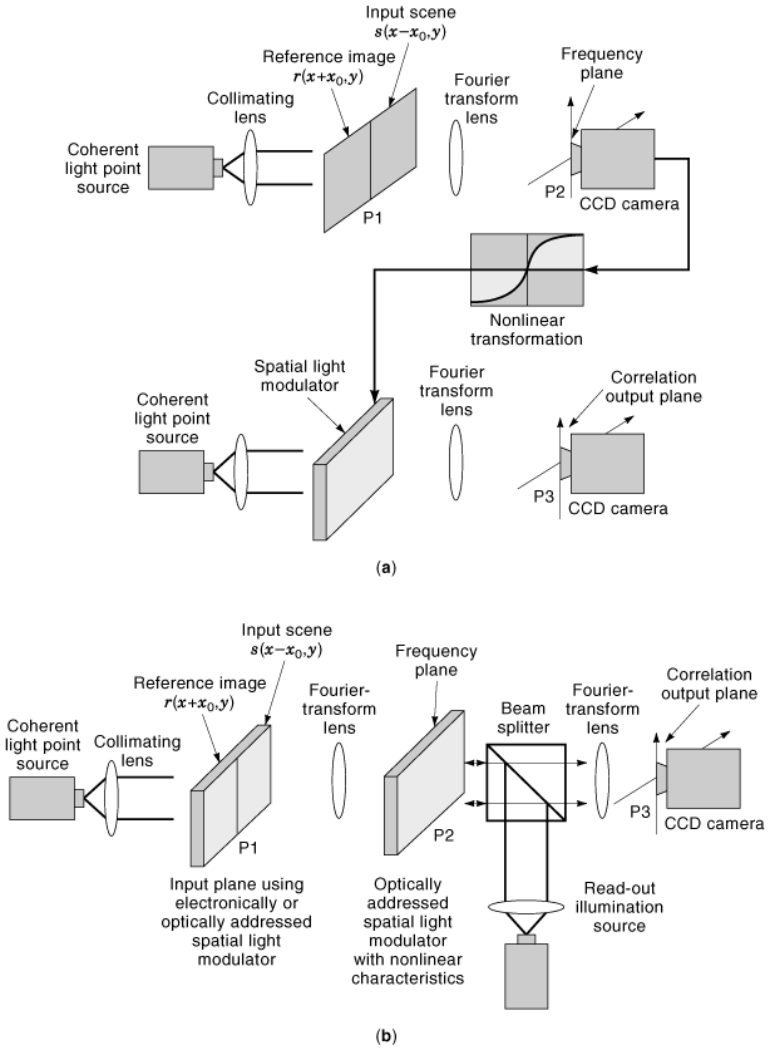

Fig. 5. Optical architecture for implementing a nonlinear joint transform correlator for image recognition: (a) Electrically addressed SLM used in the Fourier domain. (b) Optically addressed SLM used in the Fourier domain.

Another filter design approach is the joint transform correlator (1), as shown in Fig. 5. An input scene $s(x, y)$ and reference image $r(x, y)$ are presented side by side at the input plane. The input scene can be displayed on a SLM for real-time operation (see Chap. 4 of Ref. 6). Plane P1 is the input plane that contains the reference image $r(x + x_\theta, y)$ and the input image $s(x - x_\theta, y)$. The amplitude of the light distribution at the back focal plane of the transform lens FTL1 is the sum of the Fourier transforms of the two input images. We denote $S(\alpha, \beta) \exp[j\phi_s(\alpha, \beta)]$ and$_R(\alpha, \beta) \exp[j\phi\ R(\alpha, \beta)]$ as the Fourier transforms of the input and reference images $s(x, y)$ and $r(x, y)$, respectively. The Fourier transforms' interference intensity distribution $E(\alpha, \beta)$ at plane P2 is obtained using an optical sensor such as a detector array [see Fig. 5(a)] or an SLM [see Fig. 5(b)]. For the linear or classical joint transform correlator, a further Fourier transform of the Fourier transform interference intensities will produce the corss-correlation of the input and reference images at the output plane.

It is possible to design nonlinear joint transform correlators. The binary joint transform correlator is obtained by thresholding the joint power spectrum (see Chap. 4 of Ref. 6). It has been shown, both theoretically and experimentally, that binary joint transform correlators provide a higher discriminating power than the linear joint transform correlator. The binary joint transform correlator can be generalized as a family of kth law nonlinear joint transform correlators. This family includes the linear joint transform correlator for $k = 1$ and the binary joint transform correlator for $k = 0$. Here, k represents the severity of the nonlinearity of the transformation, $\text{sgn}(E_\text{m})|E_\text{m}|^k$, where E_m is the modified joint power spectrum ($E_\text{m} = E - S^2 - R^2$) and sgn ( ) denotes the signum function.

Nonlinear joint transform correlators can use a nonlinear device such as an SLM at the Fourier plane to alter the Fourier-transform interference intensity. It has been shown that compared with the linear joint transform correlator, the compression type of nonlinear joint transform correlator ($k < 1$) provides higher peak intensity, larger peak-to-sidelobe ratio, narrower correlation width, and higher discrimination sensitivity.

For a kth law nonlinearity, the Fourier transform of the correlation signal, $g(E)$, is

$$g(E) = [R(\alpha, \beta)S(\alpha, \beta)]^k \exp\{j[\phi_S(\alpha, \beta) - \phi_R(\alpha, \beta)]\} \quad (1)$$

In Eq. (1), $k = 1$ corresponds to a linear correlator and $k = 0$ corresponds to a binary nonlinearity. Varying the severity of the nonlinearity k will produce correlation signals with different characteristics. For highly nonlinear transformations (small k), the high spatial frequencies are emphasized and the correlation becomes more sensitive in discrimination. To allow for target distortion, such as rotation and scale variations, a composite reference is synthesized by using a training set of target images. For rotation-invariant pattern recognition the training set includes a number of rotated images of the target.

Many investigations of distortion-tolerant pattern recognition have been reported (1, 4, 6, 21,22,23). The performance of a nonlinear composite filter implemented by a nonlinear joint transform correlator is illustrated by Fig. 6. Two versions of a Mig29 (former Soviet Union fighter plane) target are shown in Figs. 6(a) and 6(b). A composite filter synthesized from 19 training images of a Mig29 target rotated from 0° to 90° in 5° increments is shown in Fig. 6(c). This is used as the reference image in a nonlinear joint transform correlator. Figure 6(d) shows an input scene containing two versions of a Mig29, rotated by 60° and 75°, superimposed on a background scene, then overlaid with additive noise. Mesh plots of the correlation outputs of the nonlinear joint transform correlator for $k = 0.2$ and $k = 1$ are shown in Figs. 6(e) and 6(f), respectively. It can be seen that the threshold of the response using $k = 0.2$ can be adjusted to yield the target locations, while the response using $k = 1$ cannot.

Optical computing systems can be used to process electric signals such as radar data. For example, the acousto-optic modulator discussed in the previous section can be used in a system to correlate two electric signals (12,13,14,15,16,17,18,19,20). There are two basic configurations for this; the time-integrating correlator and the space-integrating correlator. We first discuss the time-integrating correlator shown in Fig. 7(a). One input signal modulates the light-emitting diode in the far left side of the figure. The other electric signal is fed into the acousto-optic modulator as shown. The resultant product of the two signals emerging from the right-hand side of the acousto-optic cell is $s_1(t)s_2(t - x/v)$, where x is measured from the central optical axis and V is the velocity of the acoustic wave in the acousto-optic cell. Lens L1 takes a spatial Fourier transform of this in order to block the zero-order undiffracted light from the acousto-optic cell. The second lens, L2, takes a second Fourier transform and restores the spatial signal minus the dc. The light is detected by a detector, such as a charge-coupled-device (CCD) detector and if it is integrated for a time period T, the desired correlation is achieved,

$$\int_0^T s_1(t)s_2(t - x/v)\, dt$$

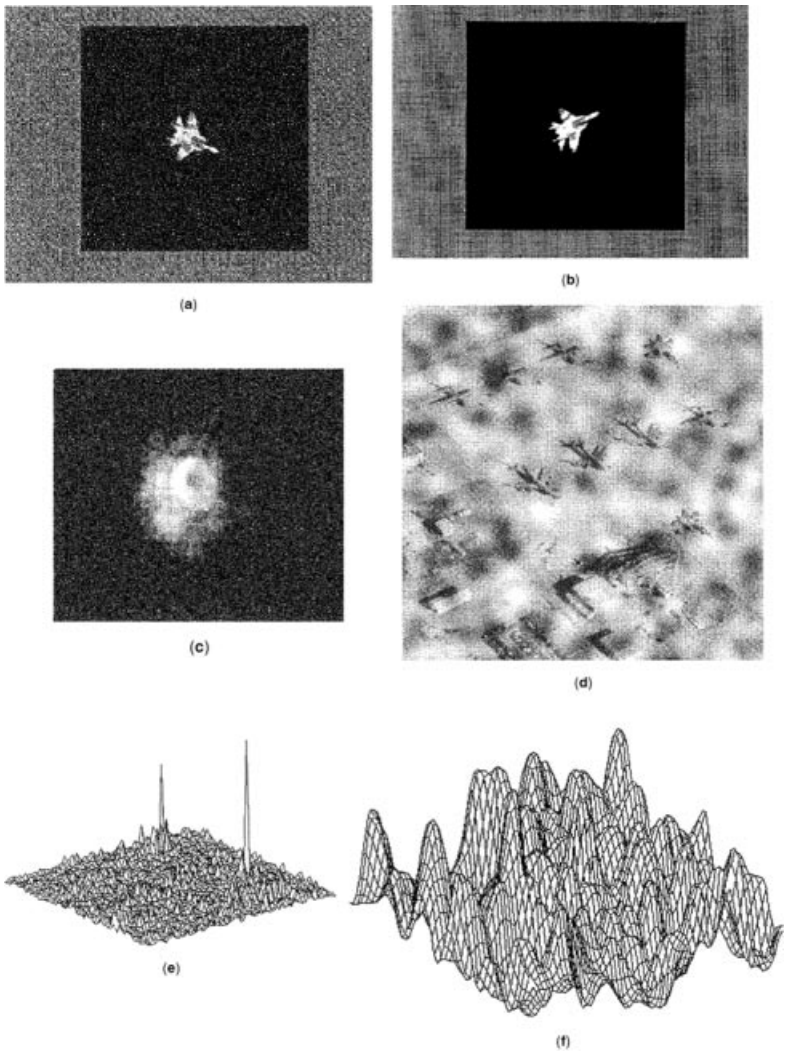

Fig. 6. Performance of the nonlinear joint transform correlator for image recognition: (a) Mig29 target, (b) Mig29 target rotated by 45°, (c) composite reference image, (d) input scene, (e) correlation output of the nonlinear joint transform correlator, (f) output of the matched filter correlator.

The other architecture commonly used is the space-integrating system, shown in Fig. 7(b). A light-emitting diode illuminates through a collimating lens the acousto-optic cell as before. In this case the two signals are fed in to opposite ends of the acousto-optic cell. This results in the two propagating waves passing each other and in effect performing the required shifting in the correlation operation. The light again goes through a Fourier transform lens where the undiffracted zero order light is blocked to improve performance by cutting down on stray light. Lens L2 retransforms the light and focuses it on to the detector. The instantaneous detector output gives a temporal profile of the correlation signal. If just the value of the correlation peak is desired, the detector can be fed to an electronic peak detecting circuit.

There are many variations of the basic schemes we have discussed here, and the reader is referred to Refs. 12–20 for more details. An architecture was proposed by Psaltis (14) that effectively makes the acousto-optic

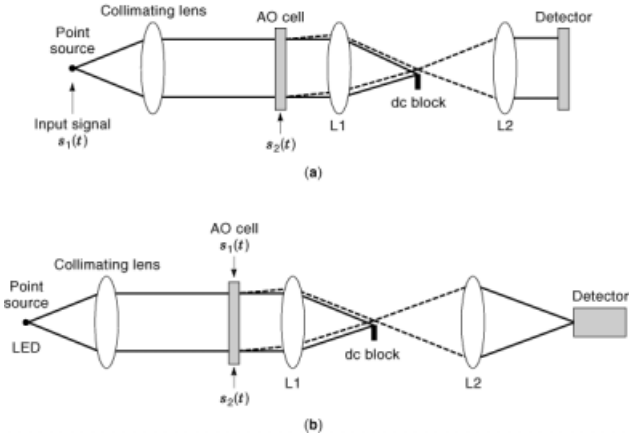

Fig. 7. Time-integrating correlator using an acousto-optic modulator. (b) Space-integrating correlator using an acousto-optic modulator.

processor a two- dimensional system capable of correlating images and therefore image recognition and target tracking. An impressive functional system using this scheme has been built and demonstrated by a group at Sandia Laboratory (see Chap. 11 of Ref. 6).

Acousto-optic cells can also be used for spectrum analysis (12, 13). The equipment consists of a light source, a Fourier transform lens, and an acousto-optic cell. A radio-frequency input from a receiver is applied to an acousto-optic cell that is illuminated by light. The acousto-optic cell separates the light into various frequency component parts in the Fourier plane. The acousto-optic cell acts as a grating where the spatial frequency of the grating is a function of the radio frequency.

Optical Encryption

Information fraud is a serious problem facing many banks, businesses, and consumers. A person may use on a daily basis several personal identification cards, credit cards, bank cards, health isurance card, driver's license, etc. Thus, there is a significant demand for fast and reliable identification of people and the verification of cards and identifications. With the rapid advances in computers, CCD technology, image- processing hardware and software, printers, scanners, and copiers, it is becoming increasingly simple to reproduce very authentic looking pictures, logos, symbols, money bills, or patterns. Recently, optical processing systems have been proposed for encryption, security systems, anticounterfeiting (26,27,28,29,30), and verification of biometrics (29, 31,32,33). Optical systems present a great potential for encryption and security applications for several reasons.

In this section we describe the use of optical information-processing systems for data encryption. Data security may be achieved by encryption to prevent unauthorized access to data. A new method of encryption proposed recently (see Fig. 8) allows one to write an encoded version of an image (two-dimensional data array) as stationary white noise (34) with a reconstruction method that is very simple and robust (27).

Let $f(x, y)$ denote an image to be encrypted. Let $n(x, y)$ and $b(\alpha, \beta)$ denote two independent white-noise sequences (34). Here x and y are the coordinates of the space domain, and α and β are the coordinates of the Fourier domain. In the encryption process, the random phase function $\exp[jn(x, y)]$ is used in the space domain, and the random phase function $\exp[jb(\alpha, \beta)]$ is used in the Fourier domain. The encrypted version of the image

can be represented as

$$\varphi(x, y) = f(x, y) \exp[jn(x, y)] * \mu(x, y) \qquad (2)$$

where $\mu(x, y)$ is the inverse Fourier transform of $\exp[jb(\alpha, \beta)]$, and $*$ denotes the convolution operation. It can be shown that $\varphi(x, y)$ is a stationary white random process. The data image can only be decrypted when the "key" $\exp[-jb(\alpha, \beta)]$, is used for the decryption.

To decrypt the image, the Fourier transform of $\varphi(x, y)$ is multiplied by the decoding mask $\exp[-jb(\alpha, \beta)]$. This causes the encoding phase function $\exp[jb(\alpha, \beta)]$ to be canceled by the decoding mask $\exp[-jb(\alpha, \beta)]$ that serves as the key for decryption. Therefore, the original data image can be recovered in the space domain by multiplying by the second phase-mask $\exp[-jn(x, y)]$. If the stored image is positive, the phase function $\exp[jn(x, y)]$ can removed by an intensity sensitive device, such as a video camera without employing the second-phase mask $\exp[-jn(x, y)]$. If the key, $\exp[-jb(\alpha, \beta)]$, is unknown and some other function is used, the image cannot be recovered and will remain a random noise. Figure 8 shows an optical implementation of the random-phase encryption. The original gray-scale image of George Washington is presented at the input plane. The encrypted version of the image is obtained at the output plane. Figure 1(c) illustrates the decrypted image using the correct keys. The encrypted image is placed at the input plane and the decrypted image (original image) is obtained at the output plane. If a wrong key is used, the recovered image will become an unrecognizable noiselike image.

We now describe a different security technique that uses complex phase/amplitude patterns that cannot be seen and cannot be copied by an intensity sensitive detector for security verification of phase encoded data (26). A composite of a phase code and biometrics such as a fingerprint, a picture of a face, or a signature are used for verification and authentication. Both the phase mask and the primary pattern are identifiable in an optical processor or correlator (1, 2, 6).

The phase portion of the pattern consists of a two-dimensional phase mask that is invisible under ordinary light. The large dimensions of the mask make it extremely difficult to determine the contents of the mask. The code in the mask is known only to the authorized producer of the card. The phase mask can be used alone. For example it can be affixed to a product and read by an optical correlator to verify authenticity. The phase mask can be represented mathematically by the function $\exp[jM(x, y)]$ where $M(x, y)$ is a real function normalized to $[-\pi$ to $\pi]$. With the high resolution of commercially available optical films and materials, $M(x, y)$ can be of the order of a million pixels, and yet the mask size will be only a few millimeters square.

A variety of techniques can be used to synthesize phase masks. The masks can be fabricated by embossing techniques on thin plastic materials, such as are used to imprint the hologram on conventional cards. Techniques such as those used to make refractive or binary optics could be employed, as well as bleaching techniques on photographic film.

The verification system that reads the card could be one of several coherent optical processing architectures (1, 2, 6). An object or primary pattern $g(x, y)$ whose authenticity is to be verified, consisting of a biometric pattern to which a phase mask has been added, is placed in the input plane of the processor. Thus the composite input signal is

$$i(x, y) = g(x, y) \exp[jM(x, y)] \qquad (3)$$

Coherent light illuminates the complex mask, extracting the signal by reflection, or the light can be transmitted through a transparent portion of the card. The processor has an a priori knowledge of the mask $\exp[jM(x, y)]$. A spatial filter may be positioned in the Fourier plane of the frequency-plane correlator to verify the code and/or the biometric. The spatial filter made for verifying the phase mask could be a variety of matched filters or spatial filters (1, 2, 6). The output correlation between the input mask pattern and the filter function is detected by the CCD image sensor. The intensity of the correlation determines the degree of similarity between

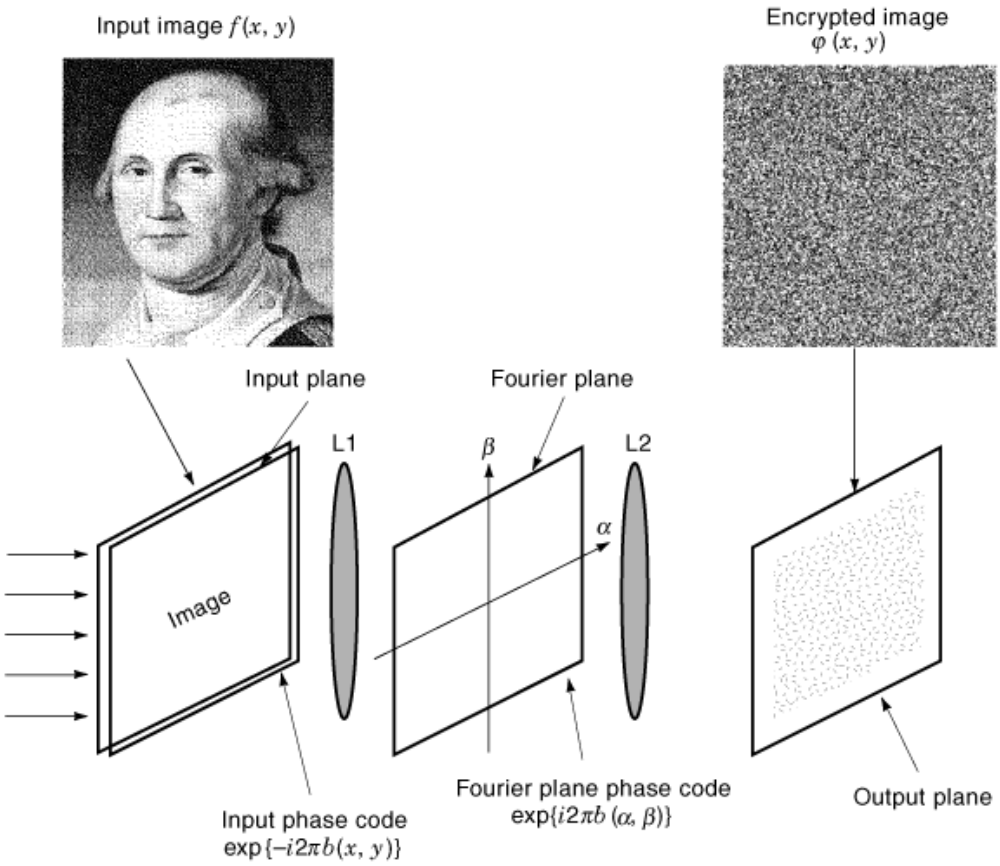

Fig. 8. Optical processing system used for optical image encryption. The input and Fourier planes have coordinates (x, y) and (α, β), respectively. The image to be encrypted is placed at the input plane. The encrypted image is obtained at the output plane. An example of the encryption of a gray-scale image is illustrated.

the input mask and the mask stored in the filter to verify the authenticity of the input phase mask on the card. If there is no primary pattern and the phase mask $\exp[jM(x, y)]$ alone is used for verification, $g(x, y)$ will be a constant. If the primary pattern needs to be verified, the processor will have an a priori knowledge of the primary pattern $g(x, y)$.

One architecture for optical correlation of objects is the joint transform correlator (JTC) (1, 6, 34) (see Fig. 5). A nonlinear JTC offers many advantages in terms of correlation performance (6, 34, 35). The input images can be displayed on a spatial light modulator (SLM) for real-time operation. Figure 9(a) shows a facial image of a person bonded onto a random phase code. Figure 9(b) presents experimental result of the verification using the nonlinear JTC when the correct facial image and random code are presented at the input of the nonlinear JTC. For even greater security, the primary pattern could itself be phase encoded (26, 31). That is, a fingerprint or picture of a face could be represented by a phase image and combined with the random phase mask discussed previously to produce a fully phase encoded key and biometrics system. This would have the effect that the combined pattern would be completely invisible to the eye or to any other detector using conventional light sources.

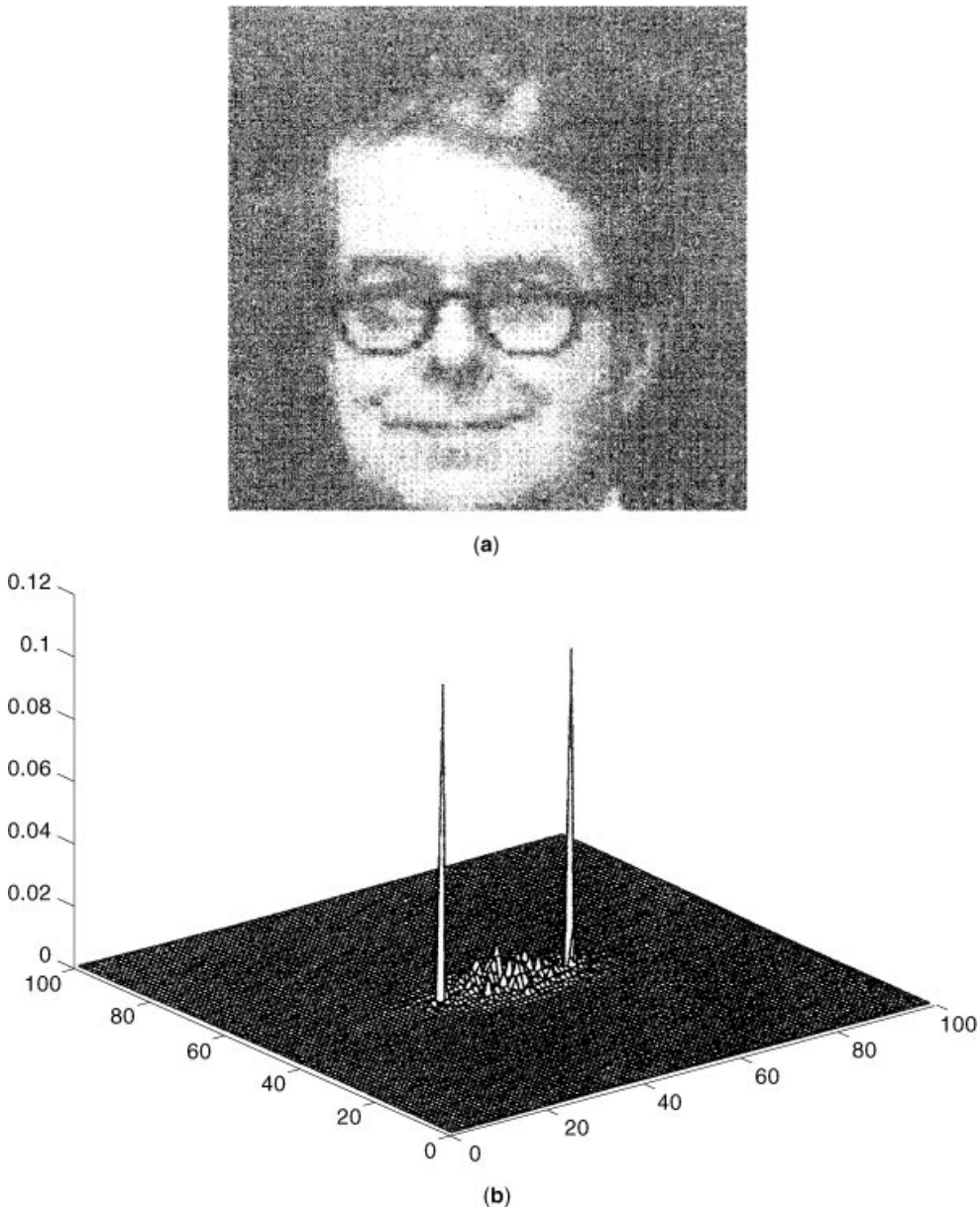

Fig. 9. (a) Person's facial image bonded onto a random phase code. (b) Experimental result of the verification using the nonlinear JTC when the correct facial image and random code are presented at the input of the nonlinear JTC.

Summary

This article has presented a brief overview of optical information-processing systems and devices. The field has made significant advances over the last 20 years with the availability of optical input–output devices or spatial light modulators for high-speed information processing, such as commercially available compact liquid-crystal

display panels with one million pixels. We have described a number of optical information processing systems for encryption, security, and identification that can be used by governments or industries that need to protect valuable data.

For more information on the topics discussed in this article, we refer the reader to the publications of the IEEE Lasers and Electro-Optics Society, the Optical Society of America, and the International Society for Optical Engineering. Each society publishes monthly journals on these topics. For example, the Optical Society of America publishes a separate monthly research journal on information processing alone. We also refer the reader to the proceedings of conferences of these societies on more specialized areas of optical information-processing devices and systems.

BIBLIOGRAPHY

1. J. W. Goodman *Introduction to Fourier Optics*, New York: McGraw-Hill, 1968.
2. B. E. A. Saleh *Fundamentals of Photonics*, New York: Wiley, 1991.
3. A. D. McAulay *Optical Computer Architecture*, New York: Wiley, 1991.
4. D. Casasent *Optical Data Processing: Applications*, Berlin: Springer-Verlag, 1981.
5. A. VanderLugt *Optical Signal Processing*, New York: Wiley, 1992.
6. B. Javidi J. L. Horner *Real-time Optical Information Processing*, Boston: Academic Press, 1994.
7. J. L. Horner *Optical Signal Processing*, Boston: Academic Press, 1987.
8. B. G. Boone *Signal Processing using Optics, Fundamentals, Devices, Architectures, and Application*, New York: Oxford University Press, 1998.
9. H. J. Caulfield *Handbook of Optical Holography*, Boston: Academic Press, 1979.
10. B. Javidi J. L. Horner Signal processing, optical, *Encycl. Appl. Phys.*, **18**: 71–100, 1997.
11. A. Yariv P. Yeh *Optical Waves in Crystals*, New York: Wiley, 1984.
12. N. Berg J. Lee *Acousto-Optic Signal Processing*, New York: Dekker, 1983.
13. D. L. Hecht Spectrum analysis using acousto-optic devices, *Opt. Eng.*, **16**: 461–466, 1977.
14. D. Psaltis Two dimensional optical processing using one dimensional input devices, *Proc. IEEE*, **72**: 962–974, 1984.
15. J. N. Lee Optical and acousto-optical techniques in radar and sonar, *Proc. SPIE*, **456**: 96–104, 1984.
16. K. T. Stalker F. M. Dickey, M. L. Yee Acousto-optic correlator for optical pattern recognition, in B. Javidi and J. L. Horner (eds.), *Real-time Optical Information Processing*, Boston: Academic Press, 1994.
17. D. Psaltis M. Haney Acousto-optic synthetic aperature radar processors, in J. L. Horner (ed.) *Optical Signal Processing*, New York: Academic Press, 1987, pp. 191–241.
18. N. A. Riza In-line interferometric time-integrating acousto-optic correlator, *Appl. Opt.*, **33** (14): 3060–3069, 1994.
19. N. A. Riza Space integrating interferometric acousto-optic convolver, *IEEE Photon. Technol. Lett.*, **7** (3): 339–341, 1995.
20. W. T. Rhodes Acousto-optic signal processing: Convolution and correlation, *Proc. SPIE*, **69**: 65–79, 1981.
21. D. Casasent Unified synthetic function computation formulation, *Appl. Opt.*, **23**: 1620–1627, 1984.
22. D. Casasent W. Chang Correlation SDF's, *Appl. Opt.*, **25**: 1032–1033, 1986.
23. D. L. Flannery J. L. Horner Fourier optical signal processors, *Proc. IEEE*, **77**: 1511–1527, 1989.
24. J. L. Turin An introduction to matched filters, *IEEE Trans. Inf. Theory*, **IT-6**: 311–329, 1960.
25. B. Javidi J. Wang Design of filters to detect a noisy target in non-overlapping background noise, *J. Opt. Soc. Am. A*, **11**: 2604–2613, 1994.
26. B. Javidi J. L. Horner Optical pattern recognition for validation and security verification, *Opt. Eng.*, **33** (6): 1752–1755, 1994.
27. P. Refregier B. Javidi Optical image encryption using input and Fourier plane random phase encoding, *Opt. Lett.*, **20**: 767–769, 1995.
28. H. S. Li Y. Qiao, D. Psaltis Optical network for real-time face recognition, *Appl. Opt.*, **32**: 5026–5035, 1993.
29. B. Javidi J. Li, Q. Tang Optical implementation of neural networks for face recognition using a nonlinear joint transform correlator, *Appl. Opt.*, **34**: 3950–3962, 1995.
30. B. Javidi G. Zhang, J. Li Experimental demonstration of the random phase encoding technique for image encryption and security verification, *Opt. Eng.*, **35** (7): 2506–2512, 1996.

31. B. Javidi A. Sergent, G. Zhang Fully phase encoded key and biometrics for security verification, *Opt. Eng.*, **36** (3): 935–942, 1997.
32. K. H. Fielding J. L. Horner, C. K. Makekau Optical fingerprint identification by binary joint transfrom correlation, *Opt. Eng.*, **30**: 1958–1961, 1991.
33. H. Rajenbach Dynamic holography in optical pattern recognition, *Proc. SPIE*, **2237**: 1329–1342, 1994.
34. B. Javidi Nonlinear joint power spectrum based optical correlation, *Appl. Opt.*, **28**: 2358–2367, 1989.
35. B. Javidi *et al.* Experiments on nonlinear joint transform correlators using an optically addressed SLM in the Fourier plane, *Appl. Opt.*, **30**: 1772–1776, 1991.

BAHRAM JAVIDI
University of Connecticut